LCLS-II Technical Note

Resonant Excitation of High Order Modes in the 3.9 GHz Cavity of LCLS-II Linac

LCLS-II TN-16-05

9/12/2016

A. Lunin, T. Khabiboulline, N. Solyak, A. Sukhanov, V. Yakovlev

1 ABSTRACT

Construction of the Linac Coherent Light Source II (LCLS-II) is underway for the world's first hard X-ray free-electron laser. A central part of the LCLS-II project is a 4 GeV superconducting radio frequency (SCRF) electron linac that will operate in continuous wave (CW) mode. The linac is segmented into four sections named as L0, L1, L2 and L3. The 3.9 GHz third harmonic cavities will be used in the section L1 of the linac for linearizing the longitudinal beam profile [1]. In this paper, we present study of trapped high order modes (HOM) excited by CW electron beam in the third harmonic cavities of LCLS-II linac. We apply statistical analysis of the eigenmode spectrum for the estimation of the probability of resonant HOM losses and influence of HOMs on beam dynamics. Furthermore, a detailed comparison of the original XFEL design and the LCLS-II design with modified End Group is performed in order to estimate the effect of reduced beam pipe aperture on the HOM damping in third harmonic cavities.

2 INTRODUCTION

A CW operation regime of the 3.9 GHz LCSL-II accelerating structure at maximum average beam current of 0.3 mA and ~1 MHz bunch repetition rate might result in significant coherent RF losses in the form of trapped HOMs [2]. Consequently, extra cryogenic losses, overheating of beam line components and unstable beam dynamic are possible deteriorating effects of a resonant HOMs excitation. The LCLS-II 3rd harmonic cavity has several modifications including a reduced beam pipe aperture of 38 mm and a redesigned HOM coupler [3]. Thus, we decided to verify the cavity performance to damp efficiently HOMs and make a comparison with the original XFEL design.

In spite of the operating mode, which is tuned separately, the parameters of HOMs vary from one cavity to another due to finite mechanical tolerances of cavities fabrication. In this paper, we use the method of generating a random cavity geometry with imperfections while preserving operating mode frequency and field flatness [4]. Based on the eigenmode spectrum calculation of series of randomly generated cavities we can accumulate the data for the evaluation HOM statistics and, thus, probabilities of resonant HOM losses. Similar procedure is described in [5] for the 1.3 GHz LCLS-II cavity, where only frequency variations are used for the evaluation of power loss. While such an approach allows simplifying calculations, it might result in a significant overestimation of resonant HOM losses, since all modes are taken for analysis with maximum shunt impedances and quality factors. On the other part, analysis using full statistical data of HOM parameters provides most accurate results but it is a time consuming operation. For that reason, for reducing a simulation time we start the cavity eigenmode analysis with its nominal geometry in order to find out frequency passbands containing HOMs with the largest shunt impedances or quality factors. Next, we proceed for statistical calculations of random cavities but only for the HOM spectrum within the given passbands. Finally, we evaluate mean and peak values of RF power radiated to the HOM couplers, estimate probable transverse kick and compare results of a resonant HOMs excitation in both LCLS-II and XFEL 3rd harmonic cavities.

3 CALCULATION OF HOM SPECTRUM IN THE IDEAL 3.9 GHZ CAVITY.

Detailed analysis of the HOM spectrum up to 10 GHz in initial designs of the 3rd harmonic cavity is presented in [6, 7] for a single resonator with perfect electric or magnetic boundary conditions at both ends.

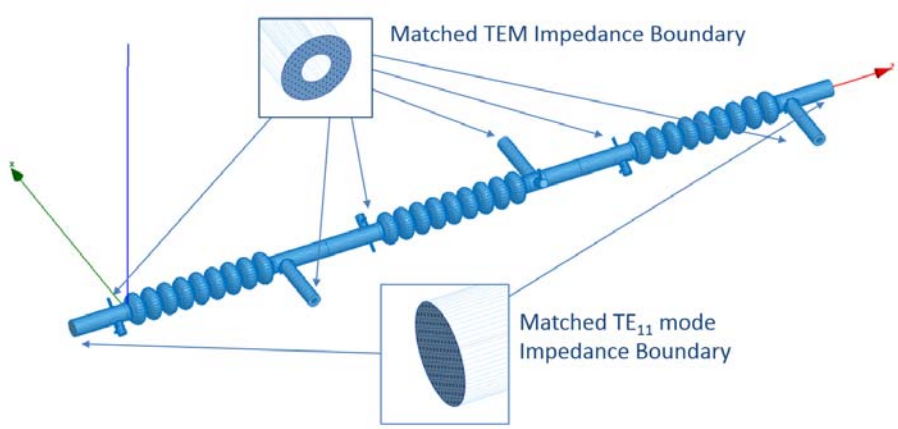

Figure 1: ANSYS HFSS model for the eigenmode analysis of the chain of three 3.9 GHz cavities.

Despite a single resonator model greatly saves eigenmodes computation time, it lacks of accuracy since the HOM parameters depend on a combination of boundary conditions. Recently new results have been published for the chain of XFEL 3.9 GHz cavities with matched boundary conditions on the coupler ports [8, 9]. Authors use chains of four and eight cavities connected together, which gives a precise evaluation of HOMs properties for propagating modes. In fact, the chain of three cavities is enough for proper calculation of the HOM spectrum and further increase of number of resonators will result in unnecessary duplication of eigenmodes and a longer simulation time. Therefore, we created the 3D model of three 3rd harmonic cavities including main and HOM couplers and field pick-up probes. The middle cavity is rotated by 180 degree according to the LCLS-II 3.9 GHz cryomodule specification. Fig. 1 shows the scheme of corresponding ANSYS HFSS project with frequency dependent matched boundary conditions to calculate the HOM spectrum up to 10 GHz.

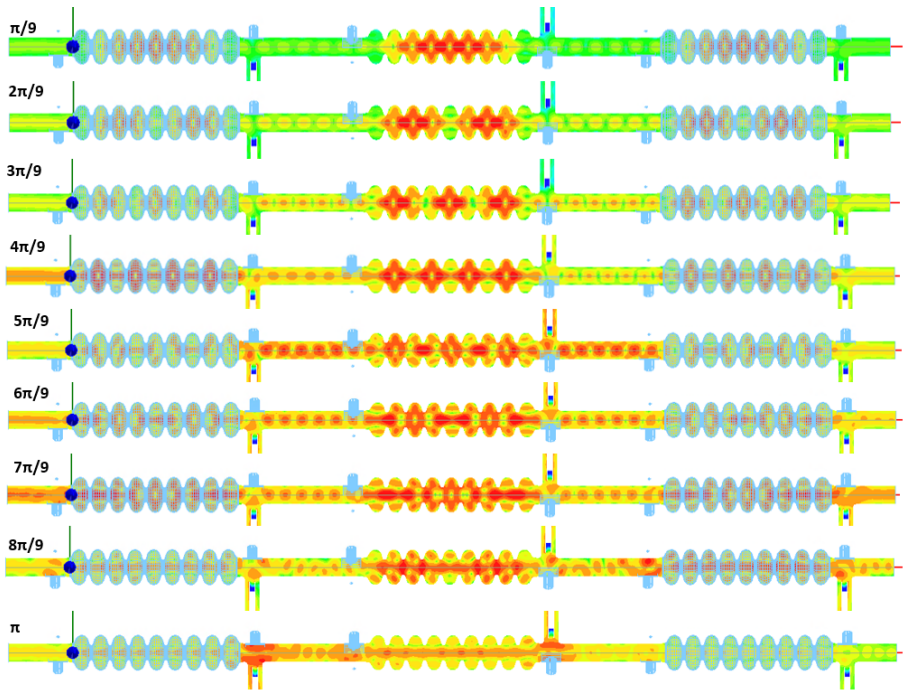

Figure 2: Distribution of electric field in the 2nd monopole band of the 3.9 GHz LCLS-II cavity (log scale)

Fig. 2 illustrates distributions of electric fields of HOMs in the 2nd monopole band in the chain of three ideal 3.9 GHz LCLS-II cavities. One can see that HOMs power is freely radiating through the coupler ports and to the beam pipe. Results of HOM parameters calculations are presented in Fig. 3 for longitudinal and transverse shunt impedances and external quality factors. We excluded spurious modes with $Q_{ext} < 100$, which appeared in simulations due to a slightly mismatch of impedance boundary conditions.

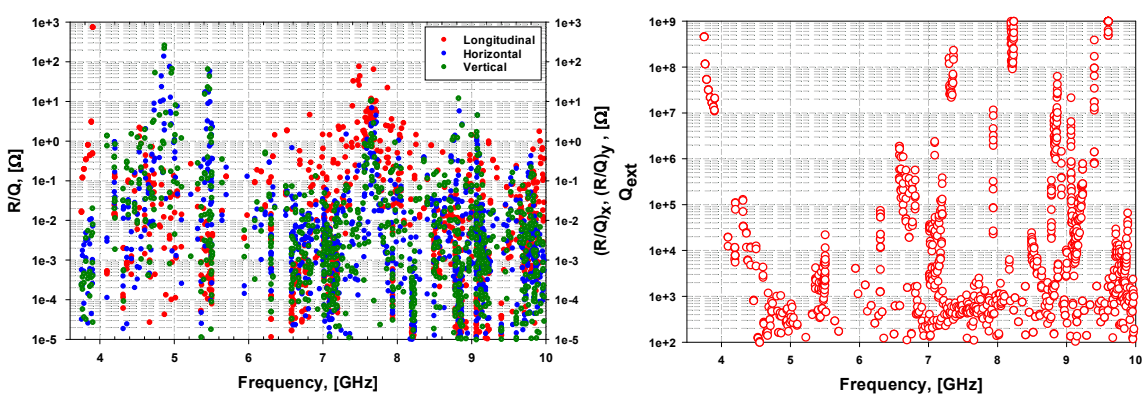

Figure 3: Parameters of HOMs, longitudinal (red), horizontal (blue), vertical (green) shunt impedances (left) and external quality factors (right), in the ideal 3.9 GHz LCLS-II cavity.

Here we use the accelerator definition of a cavity normalized longitudinal shunt impedance:

$$(R_{\parallel}/Q) = \frac{\left|\int_{-\infty}^{\infty} E_z(z)e^{ikz}dz\right|^2}{\omega_0 W}, \tag{3.1}$$

where E_z is the longitudinal component of the electric field along the cavity axis, W is the electromagnetic stored energy and ω_0 is the resonant angular frequency. Similarly, the normalized transverse shunt impedance is defined as:

$$(R_{\perp}/Q) = \frac{|U_{kick}|^2}{\omega_0 W}, \tag{3.2}$$

where U_{kick} is the transverse kick acquired by the charged particle passing through the cavity. Using the Panofsky-Wenzel theorem and the paraxial approximation for the beam trajectory, we can find the transverse kick as the transverse gradient of the longitudinal kick and, thus, calculate the transverse shunt impedance:

$$(R_{\perp}/Q) = \left|\left(\nabla_{\perp}\sqrt{R_{\parallel}/Q}\right)_{x=x_0}\right|^2 \times \frac{1}{k^2}, \tag{3.3}$$

where $k=\omega_0/c$ is a wave number. Notice that we calculate $(R_{\perp}/Q)$ at the offset of x_0 = 1 mm and the unity is Ohm.

For the CW regime, when multiple bunches pass through the cavity, the resonant high order mode excitation may occur if any of the HOM frequencies is in the synchronism with the beam harmonics. One can show that the resonant excitation results in a sum of geometrical series of individual bunch signals [10]:

$$V_{\parallel} = \sum_{n=1}^{\infty} V_0 e^{-\frac{nt_b}{\tau}} e^{i(n\omega_0 t_b + \varphi_0)} \tag{3.4}$$

where $V_{\parallel}$ is the HOM cavity voltage in the steady state regime, $V_0 = 2k_{\parallel}q_0$ is the amplitude of HOM signal excited by a single bunch, $k_{\parallel}$ is the HOM loss factor, q_0 is the individual bunch charge, t_b is the bunch spacing, $\tau = 2Q_L/\omega_0$ is the HOM signal decay time, Q_L is the HOM loaded quality factor and n is the bunch number.

For the steady state operation, the resonant gain of the HOM amplitude is expressed:

$$\left|V_{\parallel}\right|_{max} = V_0 \frac{e^{\alpha}}{e^{\alpha}-1}, \tag{3.5}$$

where $\alpha = t_b/\tau$. The average power loss due to HOM excitation can be evaluated as the energy left by the single bunch in the steady state regime over the time between consecutive bunches:

$$\langle P \rangle = \frac{1}{t_b}\left(q_0\left|V_{\parallel}\right|e^{-\alpha} + k_{\parallel}q_0^2\right), \tag{3.6}$$

where $\left|V_{\parallel}\right|e^{-\alpha}$ is the HOM voltage seeing by the bunch passing through the cavity and $k_{\parallel}q_0^2$ is the energy left the bunch itself. Finally, we can rewrite eq. (3.6) for a resonant case using the normalized longitudinal shunt impedance defined in eq. (3.1):

$$\langle P \rangle_{max} = \frac{(R_{\parallel}/Q)\omega_0 q_0^2}{4t_b}\left(\frac{e^{\alpha}+1}{e^{\alpha}-1}\right), \tag{3.7}$$

Similarly, we can derive the steady state resonant amplitude of the HOM transverse voltage if the bunch train passing the cavity off axis:

$$|V_{\perp}|_{max}^{x=x_0} = \frac{(R_{\perp}/Q)\omega_0 q_0 x_0 k}{4}\left(\frac{e^{\alpha}+1}{e^{\alpha}-1}\right), \tag{3.8}$$

Notice that both Eqs. (3.7) and (3.8) represent a general case of HOMs excitation and lead to either a non-resonant single bunch interaction regime, $\langle P \rangle = k_{\parallel}q_0^2 f_b$ if $t_b >> \tau$, or to a resonance multi-bunch cavity excitation, $\langle P \rangle = (R_{\parallel}/Q)Q_L I_0$, if $t_b << \tau$, where $f_b = 1/t_b$ is the bunch repetition rate and I_0 is the beam average current. We also skipped here the exponential form-factor $exp(-\omega_0^2\sigma_t^2)$ since the bunch time length σ_t in the L1 section of LCLS-II linac is about 3.3 ps and, hence, the bunch spectrum is much wider than the upper frequency of 10 GHz set for the HOMs analysis.

Results of resonant HOMs excitation in the ideal 3.9 GHz cavity are presented in Fig. 4 for the 0.3 mA average beam current. The most concerns cause the tens of watts of peak HOM power radiating through the

cavity coupler ports in the first monopole passband. In the following chapter, we present the detailed statistical analysis of the HOM spectrum excitation considering real cavity geometries with mechanical errors.

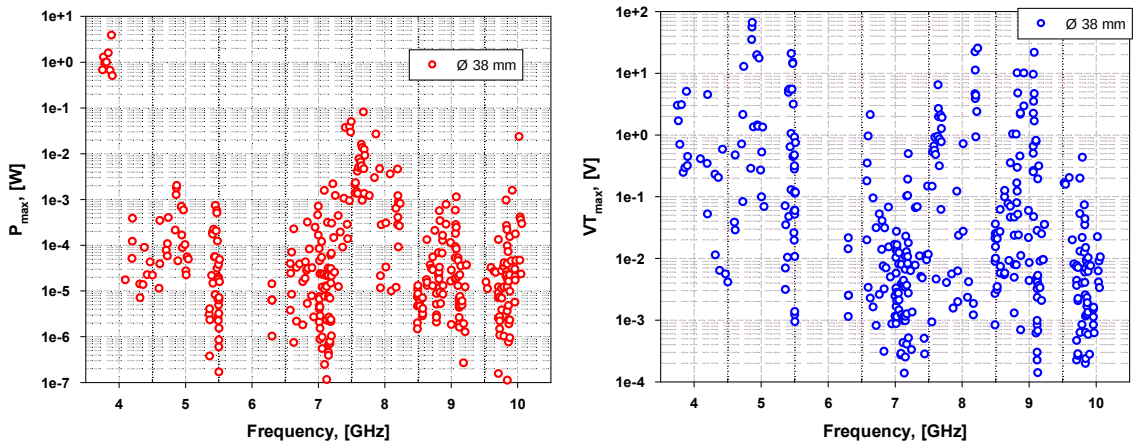

Figure 4: Resonant HOMs excitation, average power (right) and transverse voltage (left), of the ideal 3.9 GHz LCLS-II cavity in the LCLS-II linac.

4 STATISTICAL ANALYSIS OF HOM SPECTRUM IN THE 3.9 GHZ CAVITY WITH MECHANICAL ERRORS.

Conventional thin-walled niobium SRF cavities consist of multiple shell components welded together. Mechanical forming of such components and further electron-beam welding introduce significant uncertainty for the final cavity geometry. Typical deviations of cavity profiles in respect to the ideal shape are about ±200 µm and ±100 µm for 1.3 GHz and 3.9 GHz cavities respectively [11,12]. Therefore, cavities are get tuned for adjusting operating frequencies and preserving the field flatness in multicell cavities. Since each cavity has a unique geometry, the HOM spectrums vary from cavity to cavity and, then, the beam to cavity interaction has a probabilistic nature. For obtaining accurate results we apply the statistical analysis of HOM spectrum in the 3.9 GHz cavity with mechanical errors. The procedure is based on preliminary calculations of a frequency-dependent sensitivity for each of the cavity geometrical parameters [4]. Nominal geometrical parameters of the 3.9 GHz LCLS-II cavity are presented in Fig. 5. The left and right end cells are identical.

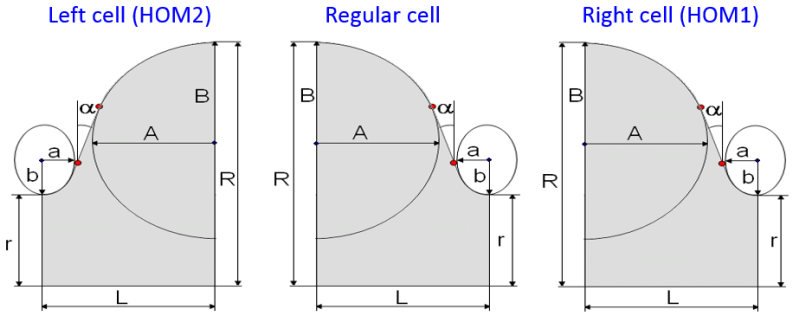

r	20
R	35.79
L	19.22
A	14.4
B	15
a	4.5
b	6.0
α	16.0

r	15
R	35.79
L	19.22
A	13.6
B	15
a	4.5
b	6.0
α	13.3°

r	20
R	35.79
L	19.22
A	14.4
B	15
a	4.5
b	6.0
α	17.4

Figure 5 Nominal geometry of the 3.9 GHz LCLS-II cavity.

Calculated frequency-dependent sensitivities are shown in Table 1 for the middle and the end half-cells. To preserve an operating mode field flatness frequencies of the half-cells are tuned by adjusting the cell

lengths similarly as it happens with real cavities. The half-cell tuning frequency balance is described then:

$$\Delta L \frac{\partial f}{\partial L} = -\sum_{n=1}^{N} \left[rnd(\sigma_{tol}) \frac{\partial f}{P_n} \right], \tag{4.1}$$

where ΔL is the compensation of the half-cell length, $\partial f/\partial L$ and $\partial f/\partial P_n$ are frequency-dependent sensitivities of the half-cell length and varying geometrical parameters, $\sigma_{tol} = \pm 100\ \mu m$ is the mechanical tolerance of a cavity fabrication. We assume here that small deviation of each parameter doesn't influence on the sensitivity of other parameters, all mechanical tolerances are the same and uncorrelated with each other.

Table 1 Frequency-dependent Sensitivities of Geometrical Parameters of the 3.9 GHz LCLS-II cavity

Parameter Name	Frequency Sensitivity, [MHz/mm]	
	Middle Half-Cell	End Half-Cell
A	-58.9	-44.5
B	19.7	16.7
a	-39.5	-8.2
b	10.2	2.5
R	-127.2	-115.9
r	51.6	18.2
L	26.2	13.1

Finally, we generated ten chains, each of three 3.9 GHz cavities with random mechanical errors. The electromagnetic simulations were done at Fermilab high performance computing servers with the ANSYS HFSS software [13,14]. Distributions of the electrical field in the chain of three cavities are illustrated in Fig. 6 for the operating monopole π-mode. Evidently the fields are split up between individual cavities due to finite tuning of the operating mode frequencies. The average calculated field flatness of the operating mode is 82%, which is close to the LCLS-II specification of minimal 90% field flatness for 9-cell cavities in the cryomodule. Figure 7 shows frequency standard deviations for modes in the first monopole band. There is a good agreement between calculations and measured 2 K data for the 3.9 GHz cavity developed for the XFEL project [15].

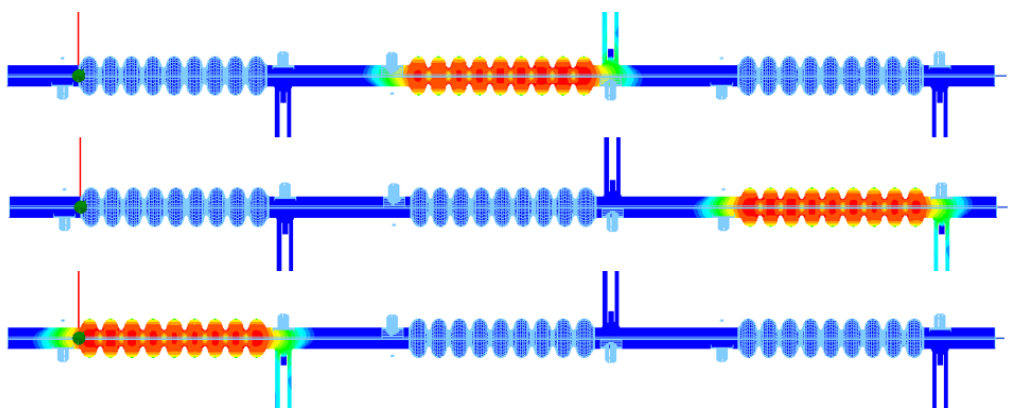

Figure 6 Operating π-mode in the chain of three 3.9 GHz cavities with mechanical errors.

For reducing a simulation time, we selected ten frequency passbands containing HOMs with most high shunt impedances and quality factors. This allows us to lower the overall number of analyzed HOMs to about five hundred comparing to fifteen hundred modes in the full spectrum up to 10 GHz. Further we filter the calculated HOM data and select only modes having more than 30% of stored energy in the middle cavity of the chain. Comparisons of HOMs resonant losses and transverse kicks in the XFEL and LCLS-II 3.9 GHz cavities are illustrated in Figure. 8. Both versions of the cavity demonstrate a similar behavior, indicating that reduced beam pipe aperture doesn't compromise the capability of HOMs damping.

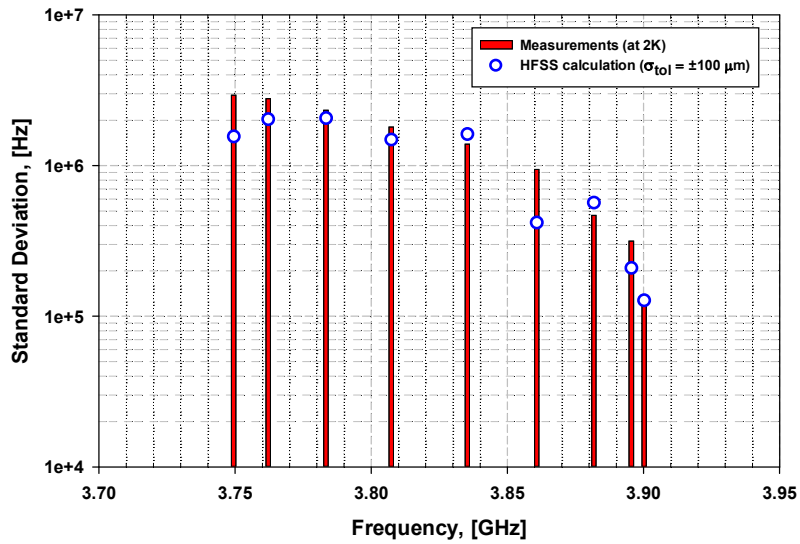

Figure 7 Frequency standard deviations for the 1st monopole band of the 3.9 GHz cavity.

The detailed analysis of resonant beam excitation of the first monopole band is presented in Figure 9, where we compare radiations of RF power to the FPC and HOM coupler ports. We plot here the average data for both upstream and downstream HOM couplers. The error bars correspond to a standard deviation of the parameters spread. In a worst-case scenario, there is up to 10 W of peak RF power radiating mostly through the FPC port. The HOM coupler ports see only a fraction of exited resonant RF power less than 0.5 W maximum. Notice that the *8π/9* mode leakage through the HOM port is heavily suppressed by the notch filter. We also don't count here the power leakage of the operating mode itself due to a finite accuracy of the notch filter tuning, which is separately estimated in [3].

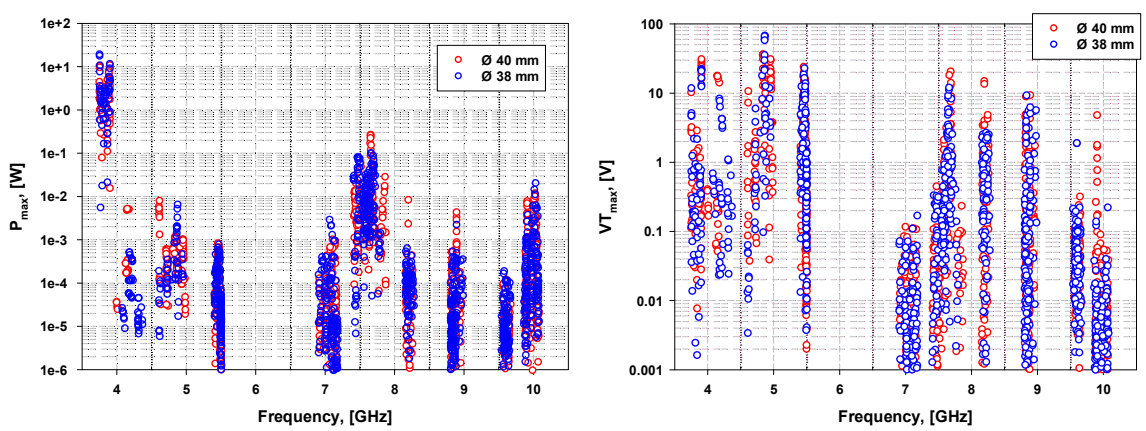

Figure 8 Resonant HOMs losses (right) and transverse kick (left) in 3.9 GHz XFEL (Ø38 mm) and LCLS-II (Ø40 mm) cavities with mechanical errors.

The resonant HOM excitation is happened only when the HOM frequency is a harmonic of the beam spectrum. The probability of such an event is very low especially in the LCLS-II linac, where the maximum bunch repetition rate is much larger than the bandwidth of most trapped resonances in SC cavities. For an accurate estimation of the probability of average HOM losses we selected 25 most dangerous HOM resonances having either the resonant power loss above 10 mW or the resonant transverse kick larger than 10 V. After filtering those modes out of the full cavity HOM spectrum we calculated medium values and standard deviations for HOMs frequencies, external couplings and shunt impedances. Results of HOMs statistical parameters evaluation are presented in Fig. 10. The high-Q resonances nearby the 8 GHz frequency are the quadruple modes. Since we don't introduce the cavity bending along the axis, the cavity geometry keeps its fully axial symmetry and these modes are trapped inside the individual cells. In reality, the cavity banding breaks the symmetry and causes coupling between quadruple and dipole modes, which effectively decreases external quality factors of quadruple modes below the 10^8 thresholds. The absence of HOMs from

the second monopole passband around 7.5 GHz is explained by their very low quality factors (<10^3) making the input to the total HOM generation negligible despite high shunt impedances.

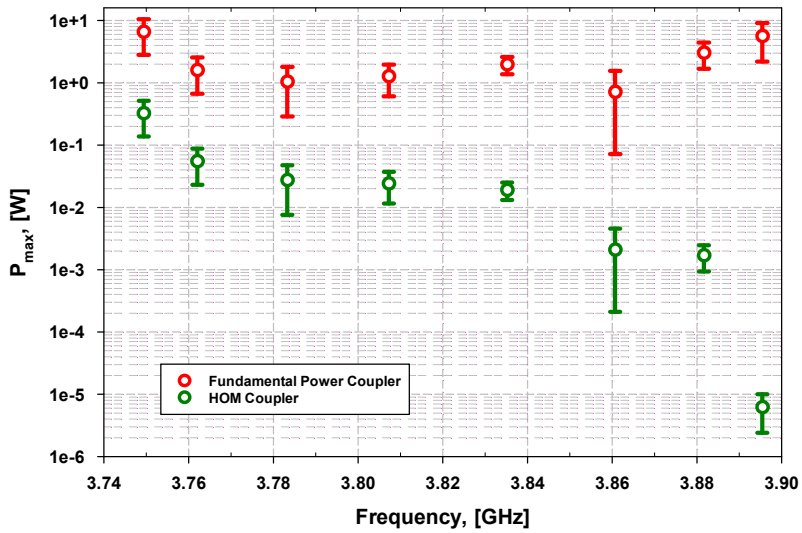

Figure 9 Resonant excitation of the first monopole band in the 3.9 GHz LCLS-II cavity with 0.3 mA average beam current.

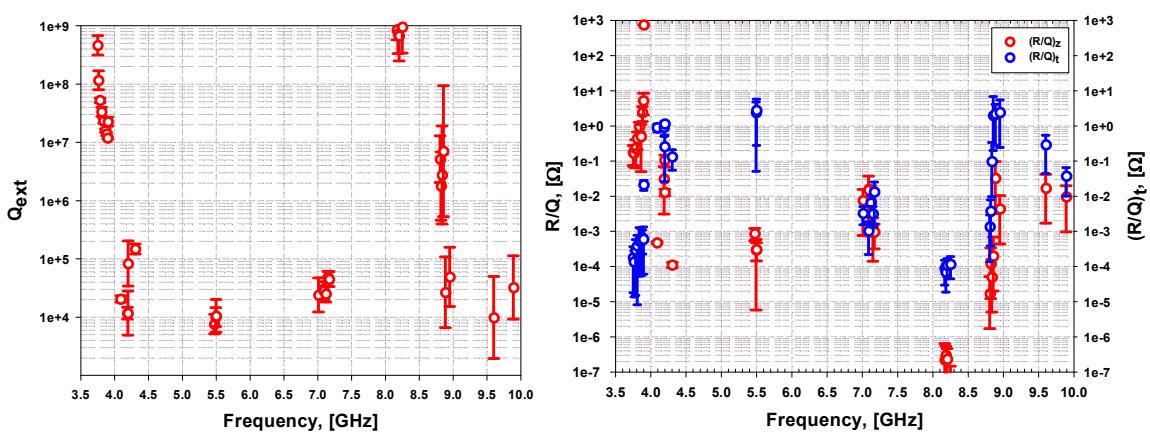

Figure 10 Spread of HOMs parameters for high-risk trapped modes in the 3.9 GHz LCLS-II cavity.

The off-response excitation of the cavity HOM spectrum is described by the same physical process given in Eq. (3.4) and the HOM amplitude gain in the steady-state regime is:

$$|V_{\parallel}| = V_0 \frac{e^{\alpha}}{\sqrt{e^{2\alpha}-2e^{\alpha}\cos(\omega_0/f_b)+1}}, \tag{4.2}$$

where ω_0/f_b is the phase difference of the HOM and the nearby beam harmonic frequencies. Corresponding average power loss and transverse kick caused by the off-resonance HOM excitation:

$$\langle P \rangle = \frac{(R_{\parallel}/Q)\omega_0 q_0^2}{4t_b} A_{\infty}, \tag{4.3}$$

$$|V_{\perp}|_{x=x_0} = \frac{(R_{\perp}/Q)\omega_0 q_0 x_0 k}{4} A_{\infty}, \tag{4.4}$$

where $A_{\infty}=2(e^{2\alpha}-2e^{\alpha}\cos(\omega_0/f_b)+1)^{-0.5}+1$ is the resonant form-factor in the steady-state regime. Finally, we seeded 10^5 random HOM spectrums and calculated the cumulative probability of HOMs losses [16] and

transverse kick in the 3.9 GHz cavity. The results are presented in Fig. 11 for 0.3 mA average beam current in the LCLS-II linac. The anticipated median value of HOMs power radiating to the FPC and HOM coupler ports is below 0.1 mW. There is a low probability (<0.1%) that the pick HOMs power larger than 1 W will be radiated to the FPC port and a negligible probability (<0.001%) of radiating power more than 0.1 W to the HOM ports. The median HOMs transverse kick is expected to be less than 100 V per cavity, while the peak value of a resonant transverse kick could be as large as 2-3 kV with the probability of ~ 0.01%.

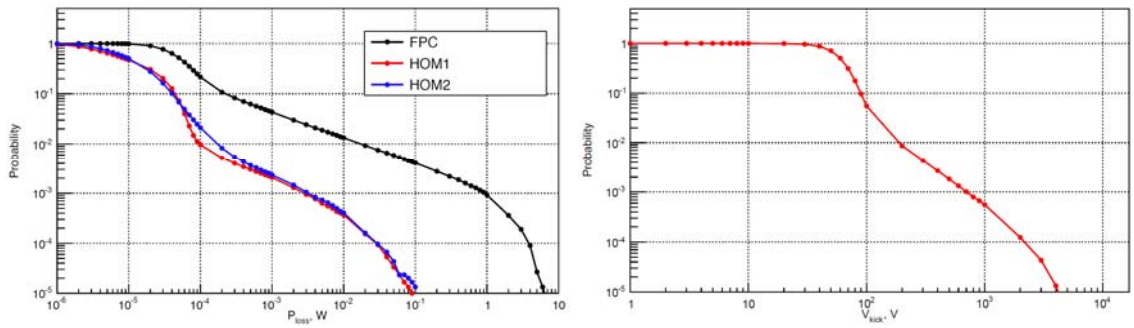

Figure 11 Cumulative probability of HOMs power loss (left) and HOMs transverse kick (right) in the 3.9 GHz LCLS-II cavity for 0.3 mA average beam current.

Eventually, we conclude that the 3.9 GHz cavity with a reduced beam pipe aperture is capable of efficiently damping the resonant excitation of HOMs spectrum by the continuous beam in the LCLS-II linac.

5. CONCLUSIONS

We performed the statistical analysis of the eigenmode spectrum up to 10 GHz in the 3.9 GHz LCLS-II cavities with reduced beam pipe aperture. The analysis is done for the cavities with typical ±100 μm surface deviation due to mechanical fabrication errors. Cavities are expected to have a low average HOM power loss and a transverse kick of 0.1 mW and 200 V respectively. Probabilities of high peak HOM losses or kicks are below the 0.1% or less. Finally, we conclude that the 3.9 GHz LCLS-II cavity is capable of efficiently damping the resonant excitation of HOMs spectrum by the continuous beam in the LCLS-II linac and, thus, the cavity design satisfies to the LCLS-II requirements.

6. REFERENCES

[1] LCLS-II Final Design Report, LCLSII-1.1-DR-0251, SLAC, 2015

[2] SCRF 3.9 GHz Cryomodule Physics Requirements Document, LCLSII-4.1-PR-0097-R2, SLAC, 2016

[3] A. Lunin, et al., "Redesign of the End Group in the 3.9 GHz LCLS-II Cavity", MOPLR007, LINAC'16, East Lansing, USA, 2016

[4] A. Sukhanov, et al., "High Order Modes in Project-X Linac", Nuclear Instruments and Methods in Physics Research Section A, Volume 734, Part A, 11 January 2014

[5] A. Sukhanov, et al., "Resonant Excitation of High Order Modes in Superconducting RF Cavities of LCLS II linac", LCLSII-TN-15-06, SLAC, 2015

[6] J. Sekutowicz, R. Wanzenberg, "A Design of a 3rd Harmonic Cavity for the TTF 2 Photoinjector", TESLA-FEL 2002-05, DESY, 2002

[7] T. Khabibouline et al., "Higher Order Modes of a 3rd Harmonic Cavity with an Increased End-cup Iris", FERMILAB-TM-2210, Fermilab, 2003

[8] L. Xiao et al., "RF Simulations for an LSLC-II 3rd Harmonic Cavity Cryomodule", THPB008, SRF2015, Whistler, BC, Canada

[9] T. Flisgen et al., "Eigenmode Compendium of the Third Harmonic Module of the European X-ray Free Electron Laser", Phys. Rev. ST Accel. Beams, to be published.

[10] F. Cullinan et al., "Long bunch trains measured using a prototype cavity beam position monitor for the

Compact Linear Collider", Phys. Rev. ST Accel. Beams, 18, 112802, 2015

[11] A. Matheisen, "Cavity Fabrication and Preparation Sequences for the TESLA/TTF Cavities at DESY", 1st ILC workshop at KEK, Japan

[12] N. Solyak et al., "Development of the Third Harmonic SC Cavity at Fermilab", PAC'03, Portland, OR, USA, 2003

[13] http://www.ansys.com/Products/Electronics/ANSYS-HFSS

[14] A. Lunin, "Status of the HPC cluster for Multiphysics Engineering Analysis", SRF Monday Meeting February 08, Fermilab, 2016

[15] T. Khabiboulline, private communications